Proceedings of the
Estonian Academy of Sciences
2025, **74**, 2, 132–136

https://doi.org/10.3176/proc.2025.2.08

www.eap.ee/proceedings
Estonian Academy Publishers

POWDER METALLURGY

RESEARCH ARTICLE

Received 28 January 2025
Accepted 26 February 2025
Available online 16 April 2025

Keywords:
high entropy, carbide, low temperature, microstructure, sintering routes

Corresponding author:
Furqan Anwar
furqananwar1201@gmail.com

Citation:
Anwar, F., Tarraste, M., Berger, L.-M. and Pötschke, J. 2025. Effect of carbon content on the microstructure and phases of (Ti,V,Nb,Cr,Mo)Cx high-entropy carbide. *Proceedings of the Estonian Academy of Sciences*, **74**(2), 132–136. https://doi.org/10.3176/proc.2025.2.08

Effect of carbon content on the microstructure and phases of (Ti,V,Nb,Cr,Mo)Cx high-entropy carbide

Furqan Anwar[a], Marek Tarraste[a], Lutz-Michael Berger[b] and Johannes Pötschke[b]

[a] Department of Mechanical and Industrial Engineering, Tallinn University of Technology, Ehitajate tee 5, 19086 Tallinn, Estonia
[b] Fraunhofer IKTS, Winterbergstr. 28, D-01277 Dresden, Germany

ABSTRACT

High-entropy carbide (Ti,V,Nb,Cr,Mo)Cx with varying carbon content (x = 13–16 wt%) was synthesized using conventional argon sintering at 1800 ˚C. Homogeneous distribution of elements was obtained at x = 15 wt% of C, while the presence of residual secondary carbide was observed among all samples with varied carbon content. Density of the high-entropy carbides increases with increasing carbon concentration. The results reveal significant changes in both the microstructure and phase composition. A precise carbon window is required to attain homogeneous distribution among the elements to form a stabilized high-entropy face-centered cubic (FCC) phase structure. Deviations from this narrow carbon window lead to the segregation of chromium in the microstructure, which in turn alters the stoichiometry of the high-entropy carbide system.

Introduction

Traditionally, materials with a highly stable structure are ceramics, such as carbides or oxides. Such materials consist of one parent and one interstitial element. Transition metal carbides are known for their elevated temperature stability and corrosion resistance. These carbides are synthesized at a temperature higher than 2000 °C. Their synthesis temperature depends on the diffusion of metal atoms to form a stable crystal while incorporating carbon within its structure at interstitial sites [1]. Transition metal carbides from periodic groups IVb and Vb consist of a face-centered cubic (FCC) close-packed crystal structure with a metal to carbon ratio of 1:1. However, in practice, there exist some vacancies in the lattice, which are due to carbon deficiency and can alter the mechanical properties of the carbide by causing phase changes and density variations [2]. Varying carbon content can alter the density of the carbide under similar synthesis conditions [3]. For example, the relative density of zirconium carbide (ZrCx) (x = 0.5–1 wt%) increased from 91% to 98% as the carbon content decreased from higher content to lower content under similar conditions. This change is attributed to the lower activation energy required in the presence of low carbon content [1].

The high-entropy carbides (HECs) consist of five or more transition metals combined with carbon. These materials possess high hardness and elevated temperature stability similar to their parent mono carbides [4]. Due to the variety of elements, HECs can have multiple phases depending on the carbon level. Since the parent element can form its own carbide, carbon plays an important role in the activation energy and atom's mobility in the HEC structure [5]. In recent studies, varying carbon content in various HECs, such as (W,Ta,Nb,Zr,Ti)Cx, (Ti,Zr,Nb,Ta,Mo)Cx, (Ti,Zr,Hf,V,Nb,Ta)Cx, had a significant effect on their microstructure, phase, density, mechanical and electronic properties [6–8]. To predict the phase composition of an HEC, various theoretical models are utilized, such as CALPHAD, entropy formation ability (EFA), and density function theory (DFT) [9]. Kaufmann et al. [10] used machine learning to calculate the EFA of various chromium-containing HECs. Their work showed that HEC compositions with an EFA lower than 55(eV/atom)$^{-1}$ result in a multiphase microstructure, mainly consisting of WC and Mo_2C as secondary carbides.

The synthesis of a single-phase HEC is influenced by the carbon concentration. Varying carbon content can help achieve an efficient route for the synthesis of the single-phase HEC. In this work, the synthesis of (Ti,V,Nb,Cr,Mo)Cx HEC is conducted, and the effect of carbon concentration (x = 13–16 wt%) is observed on the synthesis and microstructure, prepared from metallic powders through pressureless sintering. Different structure and composition characterization methods, such as energy dispersive X-ray spectroscopy (EDX), backscattered electron (BSE) imaging, and X-ray diffraction (XRD) phase analysis, are utilized to understand the phase change of the HEC in this work.

Experimental procedure

Titanium (Ti, 37–44 µm; Baoji Ziyu Metal Materials Co., Ltd.), vanadium (V, 37 µm; Hebei Suoyi New Material Technology Co., Ltd.), niobium (Nb, 4 µm; NPM Silmet OÜ), chromium (Cr, 7 µm; Pacific Particulate Materials Ltd.), molybdenum (Mo, 2.3 µm; Pacific Particulate Materials Ltd.) and graphite (C, 3.4 µm; Imerys Graphite & Carbon) powders were employed as starting materials for the synthesis of ceramics. Metal elemental powders were added in equimolar ratio. Four different carbon content levels along with equimolar metal mixtures for optimized stoichiometry were produced. Table 1 shows the sample nomenclature and weight percentage (wt%) of all elements in different samples. These compositions underwent wet (isopropanol-based) ball milling for 72 hours, with 20 mm diameter WC–Co balls at a 20:1 ball-to-powder ratio. The slurries obtained after milling were dried overnight. Green rectangular compacts with the dimensions of 22 × 6 × 6 mm were prepared under a uniaxial force of 200 MPa. For synthesis, a conventional argon sintering route was followed, with a gradual heating rate of 10 °C/min until 1800 °C under the pressure of 50 kPa. The dwell time was kept at 120 minutes, followed by cooling in the furnace.

Phase analysis of the as-sintered samples was conducted using XRD technique with a Smartlab (Rigaku) system and Cu-Kα radiation. A step-scan data acquisition with a step size of 0.02° and a diffraction angle (2θ) range of 20–80° was used. Their bulk densities were determined using Archimedes' principle. The theoretical densities were obtained using the ThermoCalc software. The microstructure of the polished samples was observed using a scanning electron microscope (SEM) in BSE imaging mode (Zeiss EVO). Elemental mapping was conducted using the EDX technique.

Results and discussion

Phase composition

XRD was performed to investigate the phase composition of the sintered high-entropy carbides. The XRD patterns of different compositions are presented in Fig. 1. There are multiple peaks in the XRD pattern, indicating the presence of secondary carbides in the structure. The formation of the FCC structure was confirmed by the presence of characteristic FCC peaks corresponding to a rock salt structure, similar to that of titanium carbide (TiC). These peaks dominate the

Table 1. Stoichiometry of equimolar metal mixtures and their corresponding carbon values

Sample name	Sample composition, wt%					
	Titanium (Ti)	Vanadium (V)	Niobium (Nb)	Chromium (Cr)	Molybdenum (Mo)	Carbon (C)
HEC-13	12.3	13.0	23.8	13.3	24.5	13
HEC-14	12.1	12.9	23.5	13.2	24.3	14
HEC-15	12.0	12.7	23.2	13.0	24.0	15
HEC-16	11.8	12.6	23.0	12.8	23.7	16

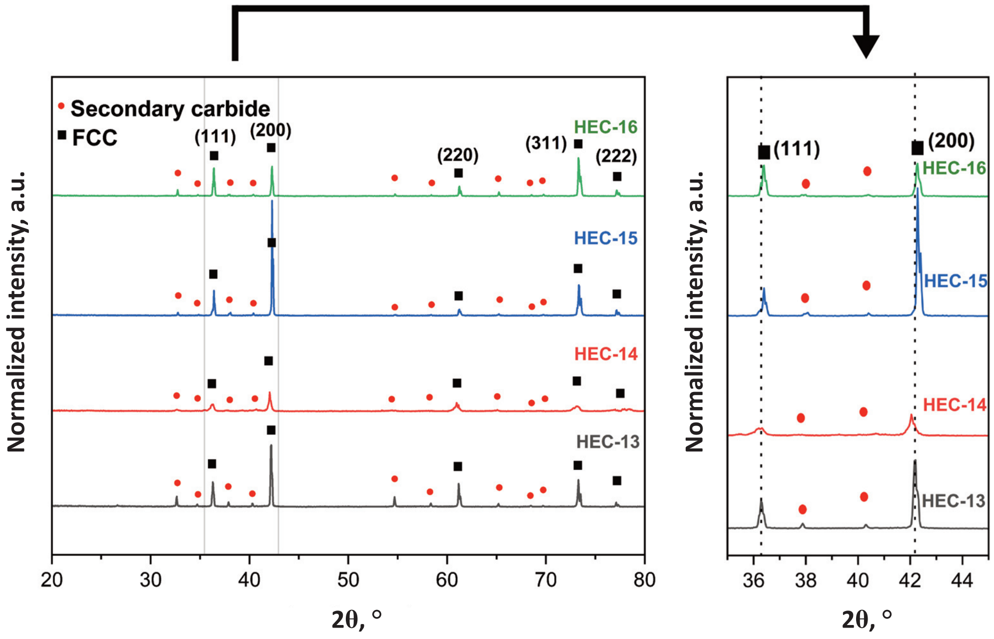

Fig. 1. XRD patterns of sintered samples at 1800 °C, showing a slight peak shift to higher angles due to the presence of secondary carbides.

Table 2. Density, grain size, and post-sintered carbon weight percentage of the fabricated samples

Sample name	Grain size, µm	Carbon (C), wt%	Theoretical density, g/cm^3	Relative density, %
HEC-13	28.29 ± 5.53	11.81	6.50	94.6
HEC-14	7.49 ± 2.78	11.30	6.50	90.3
HEC-15	33.8 ± 11.09	12.37	6.48	99.3
HEC-16	24.12 ± 3.51	11.70	6.51	97.4

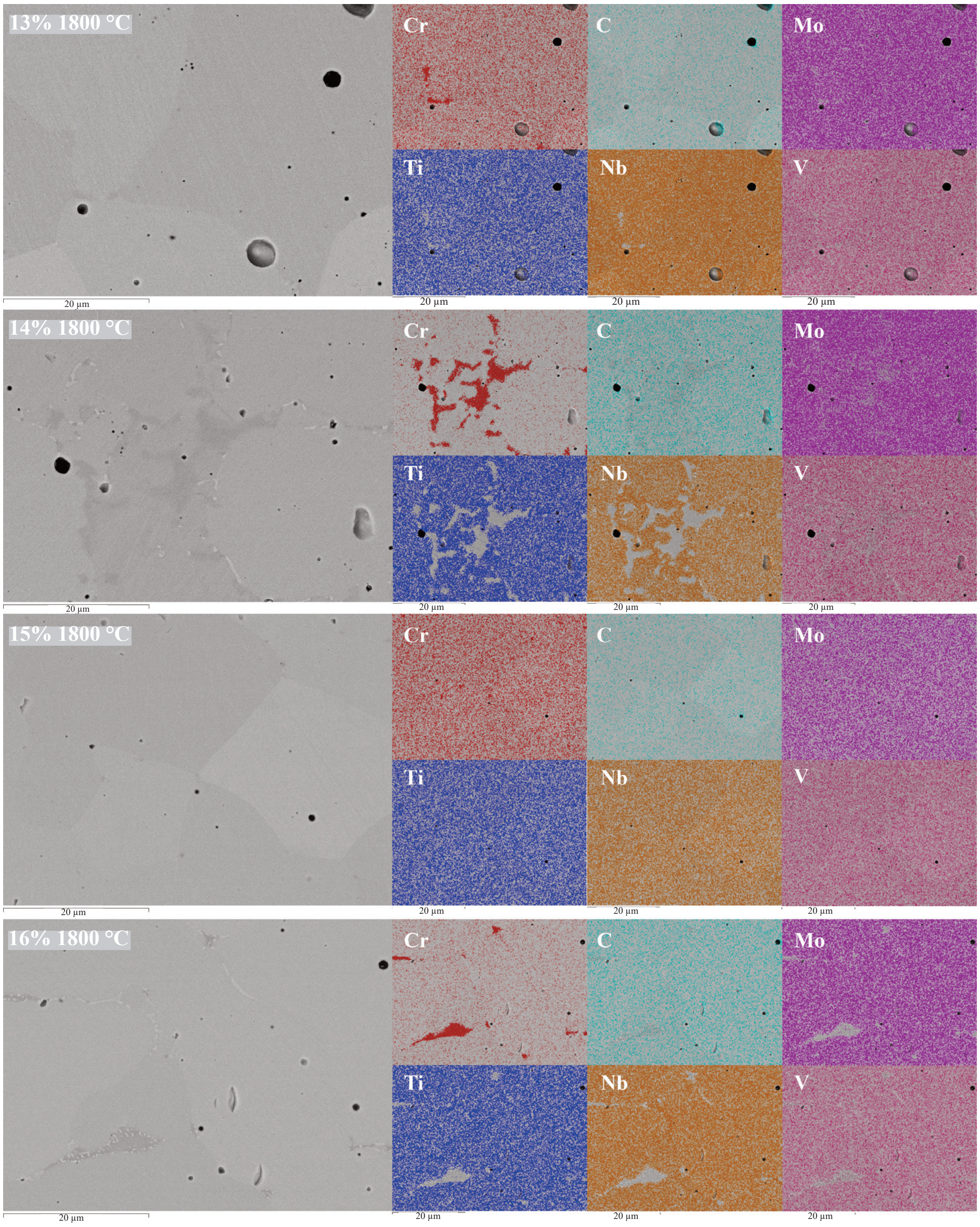

Fig. 2. SEM-BSE-EDX micrograph of sintered HEC consisting of different pre-sintered carbon percentages (13–16 wt%) at 1800 °C.

diffraction pattern in all the prepared samples. This indicates that a thermal cycle up to 1800 °C enabled the formation of the stable rock salt structure. A slight shift is observed in the FCC peaks due to the retained stress imposed by the carbon vacancies and secondary carbide phases. The smaller peaks correspond to chromium- and molybdenum-rich carbides. The presence of secondary carbides in all diffraction patterns indicates that achieving a pure FCC phase is not possible through the conventional sintering route. Kaufmann et al. [10] predicted the entropy configuration value of (Ti,V,Nb,Cr,Mo)C to be 95$(\text{eV/atom})^{-1}$, showing that a stable single-phase structure can exist for this composition.

Microstructure characterization

The relative densities of the as-sintered samples are given in Table 2. The carbon-deficient samples show poor densification, while HEC-15 with a post-sintering carbon weight percentage higher than 12% shows a maximum relative density of 99.3%. The presented micrograph in Fig. 2 shows that

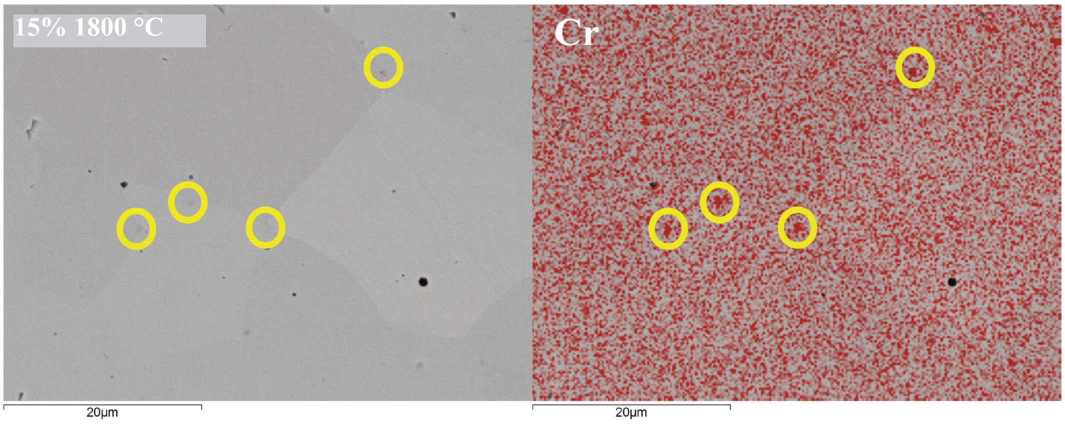

Fig. 3. SEM-BSE-EDX zoomed micrograph of HEC-15. Yellow encircled regions show chromium agglomeration.

carbon-rich samples had minor porosity in the structure, leading to a higher relative density. Elemental mapping of the as-sintered samples in Fig. 2 shows prominent chromium agglomeration in HEC-13, HEC-14, and HEC-16. Figure 3 presents the enlarged SEM-BSE-EDX micrograph of HEC-15, where encircled regions indicate chromium agglomeration, although the agglomeration level is small. In Table 2, HEC-14 has the lowest post-sintering carbon level, while HEC-15 has the highest. This indicates that as the carbon concentration in the HEC structure increases, the solubility and homogeneous distribution of elements also increase. A notable difference between the elemental mapping of HEC-15 and the rest of the composition is the solubility of Ti and Nb in HEC-15. These micrographs are consistent with the previous XRD analysis, where the secondary carbide phase is detected. Wang et al. [11] reported chromium agglomeration between the grain boundaries of (Cr,Zr,Nb,Hf,Ta)C; a similar observation is made in this work, where chromium has also agglomerated between the grain boundaries. The grain size of HEC samples in Table 2 shows that HEC-14 has a drastically smaller grain size than the rest of the samples. This has occurred due to the presence of smaller chromium-rich phases in the microstructure, which has reduced the overall grain size of HEC-14. HEC-15 with very small amounts of secondary carbides has achieved the largest grain size among all the samples. A correlation can be made with the carbon content, as it is evident from the experimental values in Table 2 that as the carbon content decreases the grain size also decreases.

Conclusion

The composition with 15 wt% carbon before sintering, along with an equimolar ratio of carbide-forming metals (Ti,V,Nb,Cr,V), resulted in a homogeneous distribution of elements in the structure with minimal chromium agglomeration. The experimentation provided an optimum post-sintering carbon value of 12 wt% suitable for the homogeneous distribution of elements. Post-sintered samples with lower carbon content failed to attain a homogeneous distribution of elements within the ceramic structure as they lacked the activation energy to form stable five-element HEC structures. The presence of secondary carbides was observed in all samples, showcasing the system's inability to form single-phase structures via the pressureless sintering route at 1800 °C.

The current work is part of ongoing research; further experimentation is required to eliminate secondary carbides through the variation of the sintering routes and environment. An extensive study is already underway to understand the mobility of atoms and the causes of carbon reduction in the structure.

Data availability statement

All research data are contained within the article and can be shared upon request from the authors.

Acknowledgment

The publication costs of this article were partially covered by the Estonian Academy of Sciences.

Refrences

1. Gasparrini, C., Rana, D.-S., Le Brun, N., Horlait, D., Markides, C. N., Farnan, I. et al. On the stoichiometry of zirconium carbide. *Sci. Rep.*, 2020, **10**(1), 6347. https://doi.org/10.1038/s41598-020-63037-0
2. Gusev, A. I., Rempel, A. A. and Magerl, A. J. Disorder and Order in Strongly Nonstoichiometric Compounds: Transition Metal Carbides, Nitrides and Oxides. *Springer Series in Materials Science*, **47**. Springer, Berlin, New York, 2001.
3. Hossain, M. D., Borman, T., Kumar, A., Chen, X., Khosravani, A., Kalidindi, S. R. et al. Carbon stoichiometry and mechanical properties of high entropy carbides. *Acta Mater.*, 2021, **215**, 117051. https://doi.org/10.1016/j.actamat.2021.117051
4. Oses, C., Toher, C. and Curtarolo, S. High-entropy ceramics. *Nat. Rev. Mater.*, 2020, **5**(4), 295–309. https://doi.org/10.1038/s41578-019-0170-8
5. He, Y., Peng, C., Xin, S., Li, K., Liang, S., Lu, X. et al. Vacancy effect on the preparation of high-entropy carbides. *J. Mater. Sci.*, 2020, **55**(16), 6754–6760. https://doi.org/10.1007/s10853-020-04471-3
6. Hu, J., Zhang, Y., Yan, D. and Li, Z. Unveiling the role of carbon vacancies in microstructure evolution and mechanical properties of high-entropy carbides. *J. Eur. Ceram. Soc.*, 2025, **45**(4), 117080. https://doi.org/10.1016/j.jeurceramsoc.2024.117080
7. Luo, S.-C., Guo, W.-M., Fang, Z.-L., Plucknett, K. and Lin, H.-T. Effect of carbon content on the microstructure and mechanical properties of high-entropy $(Ti_{0.2}Zr_{0.2}Nb_{0.2}Ta_{0.2}Mo_{0.2})C_x$ ceramics. *J. Eur. Ceram. Soc.*, 2022, **42**(2), 336–343. https://doi.org/10.1016/j.jeurceramsoc.2021.10.019
8. Zhang, W., Chen, L., Lu, W., Huo, S., Wei, B., Wang, Y. et al. Non-stoichiometry of $(TiZrHfVNbTa)C_x$ and its significance to the microstructure and mechanical properties. *J. Eur. Ceram. Soc.*, 2022, **42**(14), 6347–6355. https://doi.org/10.1016/j.jeurceramsoc.2022.07.007

9. Miracle, D. B. and Senkov, O. N. A critical review of high entropy alloys and related concepts. *Acta Mater.*, 2017, **122**, 448–511. https://doi.org/10.1016/j.actamat.2016.08.081
10. Kaufmann, K., Maryanovsky, D., Mellor, W. M., Zhu, C., Rosengarten, A. S., Harrington, T. J. et al. Discovery of high-entropy ceramics via machine learning. *npj Comput. Mater.*, 2020, **6**(1), 42. https://doi.org/10.1038/s41524-020-0317-6
11. Wang, Y., Csanádi, T., Fogarassy, Z., Zhang, B., Sedlák, R., Wang, X. et al. The role of Cr addition on the processing and mechanical properties of high entropy carbides. *J. Eur. Ceram. Soc.*, 2022, **42**(13), 5273–5279. https://doi.org/10.1016/j.jeurceramsoc.2022.06.026

Süsiniku sisalduse mõju kõrgentroopiakarbiidi (Ti,V,Nb,Cr,Mo)Cx mikrostruktuurile ja faasidele

Furqan Anwar, Marek Tarraste, Lutz-Michael Berger ja Johannes Pötschke

Kõrgentroopiakarbiidi (Ti,V,Nb,Cr,Mo)Cx, mille süsinikusisaldust varieeriti vahemikus x = 13–16 massi%, sünteesiti argooni keskkonnas paagutamise teel 1800 ˚C juures. Süsinikusisaldusega x = 15 massi% saavutati ühtlane elementide jaotus, kuid kõigis erineva süsinikusisaldusega proovikehades esines sekundaarkarbiide. Kõrgentroopiakarbiidide tihedus suurenes süsinikusisalduse kasvuga. Tulemused näitavad märgatavaid muutusi nii mikrostruktuuris kui ka faasilises koostises. Et tagada elementide ühtlane jaotumine ning stabiilse tahkkesendatud kristallvõrega kõrgentroopiafaasist koosneva struktuuri moodustumine, peab süsinikusisaldus jääma kindlasse vahemikku. Süsinikusisalduse kõrvalekalle sellest kitsast vahemikust põhjustab kroomi segregatsiooni mikrostruktuuris, mis omakorda muudab kõrgentroopiakarbiidi süsteemi stöhhiomeetriat.